DIFFERENCES BETWEEN THE ENERGY DETERMINED USING AN INSTRUMENTED STRIKER AND DIAL/ENCODER ENERGY

M. P. Manahan, Sr. [1], R. B. Stonesifer[2], T. A. Siewert[3], C. N. McCowan[3], and D. P. Vigliotti[3]
[1] MPM Technologies, Inc., 2161 Sandy Drive, State College, PA 16803 USA
[2] Computational Mechanics, Inc., 1430 Steele Hollow Road, Julian, PA 16844 USA
[3] National Institute for Standards and Technology, 325 Broadway, Boulder, CO 80305 USA

ABSTRACT

Both instrumented-striker systems and optical encoders are widely used to measure the absorbed energy in conventional and miniature Charpy tests. It has been observed that the total absorbed energy measured using these two technologies, while generally in good agreement, sometimes differs by up to 20 % (3 to 4.5 J) at low absorbed energies. This paper presents experimental evidence from high-speed photography of Charpy tests to show that the differences between dial/encoder energies and instrumented-striker energies (measured with U-hammers) can largely be explained by post-fracture collisions with the striker. However, experimental and numerical studies show that the vibrational energy of the pendulum and striker as well as load-cell errors due to contact-load distribution and inertial effects also contribute significantly to the differences in the measured energies.

Experimental evidence from the literature, which was originally expected to show the significance of residual vibrational energy in the test machine, may actually show that the behavior of low-energy Charpy specimens can be significantly affected by the design of the test machine. A simple dynamic model of a specimen and test machine system shows that an increase of 20 % in the stiffness of the striker and hammer assembly can lead to a decrease of 9 % in the energy required to fracture a low-energy Charpy specimen.

KEYWORDS: absorbed energy, Charpy, encoder, instrumented impact test, vibration.

RESIDUAL VIBRATION ENERGY IN A PENDULUM

Although the pendulums of dynamic test machines and their support structures are designed to be as rigid as practical, they are never perfectly rigid. This means that an impulse load applied to the pendulum will result in elastic deformations in the machine components. Once the impulse load is removed, these elastic deformations are converted back and forth between kinetic energy and elastic strains as the pendulum rings. Eventually, this energy decays through kinetic (vibrational) energy loss mechanisms. Note that the pendulum's rigid-body motion is not included in the kinetic vibrational energy. Also, while the magnitudes of the strain energy and vibrational kinetic energy components oscillate with time, their sum (i.e., the total vibrational energy) remains essentially constant with time (decays very slowly) once the pendulum is no longer in contact with the specimen. The ultimate source of the

pendulum's vibrational energy is the initial potential energy of the pendulum; therefore the energy that is either indicated by the machine's energy dial, or inferred from an optical encoder, includes any pendulum vibrational energy. Energies computed by integration of the forces determined from the striker load-cell do not include vibrational energy left in the pendulum since the integration of the force-deflection data provides the work done on the specimen over the few milliseconds required for the specimen to undergo fracture.

Finite-element simulations in a previous study calculated how much energy is left in the pendulum of a 400 J U-hammer Charpy test machine in the form of residual vibrational energy [1]. The purpose of the finite-element study was to determine how much difference one could expect between the energies measured from the dial/encoder (dial or optical encoder measurements of the pendulum travel) and from an instrumented striker (integrated load-time records from the striker) due to the effect of residual vibrational energy. In the simulations of pendulum vibration, impact loading included idealized half-sine wave impulses with periods ranging from 3 μsec (150 kHz) to 5000 μsec (0.1 kHz). Actual histories of instrumented-striker-force versus time from tests on the three ranges of National Institute of Standards & Technology (NIST) verification specimens (low-energy specimens ~16 J, high-energy specimens ~101 J, and super-high-energy specimens ~217 J) were also simulated. The simulations included strike positions at the nominal center of percussion (CP), 1 % above the CP, and 0.57 % below the CP. Residual vibrational energies in the pendulum were calculated to be within the range of 0.07 to 2.9 J. The residual energies generally depended very strongly on both the impulse's duration and the strike location relative to the CP, as seen in Figure 1. A local maximum in the residual vibrational energy was found for a pulse of about a 30 μsec (~17 kHz). For pulses in the range of 100 to 500 μsec (1 to 5 kHz), both the residual vibrational energy and its dependence on strike position reached a local minimum. This local minimum in vibrational energy is fortuitous since it coincides with the range of impulses found in transition-temperature testing of typical pressure-vessel steels. These simulations predict residual vibrational energies in the pendulum of 0 to 1 J, with perhaps as much as 2 J for some high-energy specimens. It was concluded that the pendulum's residual vibrational energy is a significant factor in the observed differences between the dial/encoder and striker energies.

In the present study, the magnitudes of vibrational energies were confirmed experimentally for strikes very near the center of percussion. The approach used was to mount accelerometers at various locations on the pendulum and hammer. Accelerations were recorded during tests on the three levels of specimen energies. Converting the acceleration data into vibrational energy involved calculating the fundamental vibration modes of the pendulum, then developing analytical models to relate the accelerations, strain energies, and kinetic energies for each mode. Two analytical models were developed. The first used accelerations measured at the mid-length of the pendulum's tubular arm, and explicitly included strain and kinetic energy associated with flexing of the arm. The vibrational energy of the U-hammer's mass was implicitly included through use of effective arm-length and mass parameters that were chosen based on matching fundamental frequencies and mode shapes from a finite-element modal analysis of the pendulum. The second model used accelerations measured on the U-hammer to calculate kinetic energy ($I\omega^2/2$) of the U-hammer's mass due to its angular vibrations. This model served primarily as an independent check on the first model's results and is considered less accurate and more sensitive to analytical assumptions (e.g., the position of the axis of rotation used for calculating the mass's moment of inertia and for relating the measured accelerations to the angular velocity).

The accelerometer data were subjected to a Fourier analysis so that accelerations could be associated with each fundamental mode of vibration. The vibrational energy was then calculated for each mode and summed to get the total vibrational energy. The results of the vibrational energy experiments are summarized in Table 1. Vibrational energies estimated from the model of the tube's lateral vibrations ranged from 0.16 J to 0.47 J. The higher-energy Charpy tests produced larger vibrational energies. The vibrational energy was computed to be between 0.2 % and 0.7 % of the measured Charpy energy, with larger fractions of vibrational energy found for the lower-energy specimens. Estimates of vibrational energy based on the U-hammer angular vibrations were nearly identical to those from the lateral-vibration model for the lowest-energy Charpy specimen. For the higher-energy specimens, the energy estimates were somewhat higher than those from the lateral-vibration model (0.95 and 2.20 J). For the U-hammer machine of this study, it appears that vibrational energies approach, but do not exceed, 1 % of the Charpy energy. The vibrational energy for the high- and super-high-energy specimens appeared primarily in the lowest-frequency vibration mode (136 Hz). The vibrational energy for the low-energy specimens appeared primarily in the third or fourth harmonics (1224 or 2175 Hz).

DISTRIBUTION OF STRIKER LOAD-CELL FORCE AND INERTIA EFFECTS

Building load cells into the strikers of dynamic test machines involves solving two fundamental problems that are generally not an issue in more typical commercial load-cell designs. The first and most important is the ability to accurately measure loads that are applied and removed over a time scale of microseconds. The other is the ability to modify a striker geometry to improve its performance as a dynamic load cell, without compromising its performance as a striker. Finite-element simulations were used in a previous study to estimate the responses of instrumented-striker load cells [1]. A key issue was the sensitivity of the striker's load cell to variations in the distribution of the contact force between the Charpy specimen and the striker.

There are numerous reasons why the contact force can move differently between calibration specimen and test specimen, between test specimens, and during a test on a single specimen. Some of these factors affect the horizontal distribution of load, while others affect the vertical distribution:

1. elastic deformations of the striker and pendulum (vertical)
2. rotations of the striker due to pendulum's rigid-body rotation (vertical)
3. specimen machining tolerance of 10 minutes on squareness (vertical)
4. wear of the striker, anvils, or supports (horizontal and vertical)
5. plasticity in the specimen, leading to redistribution of the force and loss of contact at the specimen's edges (horizontal and vertical)
6. wrapping of the specimen around a wide (radius of 8 mm) striker, with plowing of the specimen surface and associated pinching of the striker nose (horizontal)
7. specimens of different material and therefore different elastic and plastic behavior (horizontal and vertical)
8. differences in specimen height (e.g., miniature vs. full-size specimens) (vertical)
9. asymmetry in crack growth (horizontal and vertical)

Finite-element simulations of variations in the bounding horizontal load on striker with a nose radius of 8 mm showed a maximum load-cell error of 1.2 % [1]. Simulations of variations in the vertical load showed a much larger potential for error in the load-cell than was associated

with variations in the horizontal load. Bounding distributions where all of the load was concentrated at either the top or the bottom edge of the specimen led to load-cell errors as great as 45 % from when the load cell was simulated as being calibrated with a uniform contact pressure. Although the distribution of realistic contact loads is not well known, this study suggested that load errors as large as 8 % might be expected at some typical loads.

The effects of variations in the simulated load [1] are entirely consistent with those found through the simulations of Kobayashi et al. [2]. They found that load errors on the order of 10 % can be expected if a test is done on an aluminum specimen after calibration using a steel specimen. They also found that calibration with a specimen 10 mm thick and then testing a specimen 2 mm thick could lead to load errors on the order of 10 %. Although they do not clearly state that the load-cell errors are due to changes in the distribution of the load on the striker, this is clearly an explanation for their observations. They reasonably conclude that an instrumented-striker system must be calibrated for each new specimen material or specimen size. They do not broach the subject of changes in the distribution of the contact force that can occur within a single test due to plasticity or striker rotation. Kalthoff et al. [3] studied the effects of load distribution on strikers of 2 mm and 8 mm radius. They considered only effects of the distribution of loads in the horizontal direction and focused on the effect that wrapping of the specimen around the striker at large deformations could have on load-cell accuracy. They found load-cell errors as large as 10 %, with titanium strikers being more prone to error than steel, and the design with the 8 mm radius being more prone to error than the design with the 2 mm radius. The sensitivity to horizontal load distribution for the results from the striker with 8 mm radius [1] is consistent with the ±1 to 2 % (steel striker with strain gages on the sides) of [3]. Winkler and Voβ [4] report experiments that show that variations in the load distribution cause as much as a 5 % error for a load cell with a striker of 8 mm radius. They considered variations due to wear or small permanent deformations in the calibration specimen and/or striker. These led to different distributions of the contact force and different calibration factors with subsequent calibrations and with different levels of calibration force. The 8 % estimate of load distribution effects reported above for a typical test (intended to be conservative) is consistent with the 5 % calibration-related error of Winkler and Voβ.

The study by Manahan and Stonesifer [1] of the sensitivity of the striker load cell to the load distribution showed that the elastic rotation in the striker contact-surface during a typical test is similar in magnitude to the requirement of a 10-arc-minute squareness in the ASTM E23 standard, and so justifies this squareness tolerance. Very high-energy Charpy specimens can be in contact with the striker for as much as 1 to 2 degrees of pendulum rotation. At a rotation of 2 degrees, the striker on a typical 400 J machine will have displaced the bottom edge of the specimen by about 0.35 mm more than the top edge. This top-to-bottom asymmetry would appear to cause a larger portion of the applied load to be applied to the bottom half of the specimen during a significant portion of the test duration. It also seems likely that the asymmetry would be greatest after the peak load, since the increasing loads and associated plasticity prior to peak load would be more effective at preserving top-to-bottom symmetry in the distribution of the contact force. The problems that arise from this uneven distribution of the striker load can be addressed through design optimization and calibration procedures. Descriptions of some design optimization and calibration procedures are presented in Reference [5].

It is clear from the studies reviewed above that one source for differences between dial and instrumented-striker energies is load measurement errors. Unfortunately, this is not the

only potentially significant source of load-cell errors. Another source is inertial effects. Striker load cells are often calibrated under a static load and it is inherently assumed that the strains in the load cell will be the same under dynamically-varying loads as under the static-calibration load. Manahan and Stonesifer [5] used finite-element simulations to explore the importance of inertial effects on striker load-cell accuracy. The first basic conclusion was that inertial effects and their related load-cell errors increase as the distance between the striker surface and the strain gages is increased. The second was that the error magnitudes depend very strongly on the rate of change of the applied load (i.e., pulse duration or frequency). One set of simulations aimed at quantifying the potential error for magnitudes of the peak loads in typical pressure vessel materials produced error estimates for gages placed at 8 mm, 14 mm, and 27 mm from the striking surface. The error was doubled when going from 8 to 14 mm, and then doubled again when going from 14 to 27 mm. The inertia-related error at the 8 mm gage placement was in the range of 2 to 5 %, depending the amount of plasticity exhibited by the specimen before reaching the peak load.

The incremental work done on a specimen is proportional to the force applied. Therefore, errors in load measurement should lead to differences in dial and instrumented-striker energies. Load-cell errors due to inertial effects were found to oscillate greatly in numerical simulations. Since calculating the energy from the force signal involves integration, it seems reasonable to expect this oscillatory inertia-related error will be reduced as the integration combines measurements over the entire cycle. However, this may not be the case, as shown by Manahan and Stonesifer in [1]. Obtaining energy from the striker force record requires that the specimen displacement versus time history also be known. The usual approach in determining displacement is to calculate the deceleration of the striker based on its known mass and the measured force, and then to integrate the accelerations twice with time to obtain the record of displacement versus time. Finite-element simulations [1] showed that inertial effects can produce such inferred displacements that differ from actual specimen displacements by as much as 10 % to 20 %. The displacement effect on the resulting integrated Charpy energy was 0.4 to 1.3 J when striking at the CP, and 0.5 to 2.4 J when striking within 1 % of the CP. The energy errors tended to be even larger when stopping the integration at peak load (1.2 to 1.8 J striking at CP). These calculations of energy differences assumed no load-cell errors. If load-cell errors had been included, the displacement and energy errors would be expected to be still larger.

ENERGY ASSOCIATED WITH POST-FRACTURE IMPACTS

Instrumented-striker measurements were made at NIST with simultaneous high-speed photography. The high-speed photographs (3000 frames per second) recorded the impact event and subsequent interaction with the striker. The camera was positioned either in front, or behind, the test machine so that the specimen/striker interaction could be viewed from both perspectives. Standard Reference Materials (SRMs) 2092 (low-energy range of 12 – 20 J), 2096 (high-energy range of 88 – 115 J), and 2098 (super-high-energy range of 210 – 224 J) were tested. The focus of this investigation was on characterizing the post-fracture interaction between the specimen and the striker so that the energy associated with post-fracture impact of the specimen halves with the striker could be quantified.

Over 50 high-speed films were generated simultaneously with the instrumented striker/optical encoder signals. Depending on the test temperature and alloy, specimens either

exited the back of the test machine (opposite the striker direction) or the front (direction of striker motion). Five categories of post-impact behavior were observed:

1. Specimen halves initially propagate away from the striker in a direction normal to the crack plane, and exit the rear of the test machine without striker interaction.
2. Specimen halves undergo rotation, impact the anvils and exit the rear of the test machine without striker interaction.
3. Specimen halves undergo rotation, hit the rear of the striker, and either exit the rear or fall down on the support pedestal.
4. Connected or unconnected specimen halves exit the front of the test machine having one or more post-fracture impacts with the striker.
5. Connected or unconnected specimen halves exit the front of the test machine without interaction with the striker.

During the first round of tests, a qualitative correlation was developed between the number of post-fracture hits and the energy difference between the encoder and instrumented-striker energies. In all of the tests in the low-energy range, the energy from the instrumented striker data was less than that from the dial, and this difference was observed to be larger in cases where there were multiple post-fracture impacts with the striker. The best agreement between the two values for energy (typically within about 1 %) was obtained for the higher-energy tests where the specimen exits the front of the test machine still connected and with no interaction with the striker. Good agreement was also obtained for low-energy specimens when the broken halves exit the rear of the test machine without contacting the striker. The largest differences occurred when the broken test specimens rebounded off the anvils and/or the test machine exit channel (characteristic of U-hammer test machines) and hit the striker. There were many cases where the test specimen rebounded several times off the exit channel and striker. It is interesting to note that the exit channel, which is typically constructed from low-strength carbon steel, has indentation marks from specimen interaction. The accumulation of these indentations can be detrimental because they can enhance the interactions between the exit channel and the specimens.

Two more sets of tests were performed to quantify the magnitude of the energy difference. The results are shown in Tables 2 and 3. The first set of tests was conducted at 20 °C using specimens, that fracture completely, but that may leave the machine in either direction. The tests conducted at 20 °C shown in Table 2 strongly favored the front exit. The few specimens exiting the rear either had no interaction with the striker or at most had one minor glancing-type contact where a rebound from the striker was not apparent. In contrast, all of the specimens exiting the front had numerous rebounding-type impacts with the striker. These data show that the post-fracture impacts with the striker associated with front-exiting specimens add an average of 2.9 J to the dial energy (2.3 J standard deviation). Additional tests were then conducted with the same material at –40 °C to obtain a higher fraction of rear-exiting specimens, with the results shown in Table 3. These experiments indicated a slightly higher energy due to post-fracture interactions, 4.6 J (3.3 J standard deviation). Overall, these experiments show that post-fracture interactions between the specimen and the striker can account for a large share of the energy difference between the dial and the instrumented-striker energies.

EXPERIMENTAL STUDIES FROM THE LITERATURE

ASTM Instrumented/Miniaturized Round Robin Test Program

Results from a round robin test program to compare Charpy energy test results obtained by different laboratories were compiled and reported by Manahan et al. [6]. Standard Charpy V-notch (CVN) and miniature (half-scale) Charpy V-notch specimens (MCVN) were included in the study. Instrumented strikers were used to obtain records of load versus time. The key loads were reported along with striker-based energies, as well as dial/encoder energies. The round robin used material from a previously characterized ASTM A533B Class 1 plate and two varieties of AISI 4340 steel prepared by NIST using methods similar to those used to prepare specimens for certifying Charpy test machines. For the room-temperature tests, one 4340 material and the A533B material exhibited ductile-to-brittle transitional behavior, and the other 4340 material exhibited upper-shelf behavior. At the other test temperature of 150 °C, the A533B material was well onto its upper shelf. Each participating laboratory received six specimens for each of the four material, specimen sizes, and test temperature combinations. All of the miniature specimens exhibited upper-shelf behavior due to a larger-than-expected effect of specimen size on the transition temperature. Five laboratories provided CVN data and four provided MCVN data. The machine capacities for CVN testing ranged from 300 to 368 J. The machine capacities for MCVN testing ranged from 15 to 400 J, with the 15 J machine's capacity increased to 50 J by adding weights.

The results of this ASTM round robin were examined as part of the current study to see whether there was a statistically-significant difference between the reported instrumented-striker energies and the dial/encoder energies. As described above, differences could be due to residual vibrational energy in the pendulum, to load errors (due to contact force distributions being different in the test from those during calibration), or perhaps to other unknown causes.

The dial/encoder energies agreed with the instrumented-striker energies to within ±5 % for CVN tests above 40 J. For CVNs with energy below 40 J, the agreement was within ±18 %. All the MCVNs had energies below 40 J and were in agreement to within ±12 %. Since there were six duplicate tests for each combination of material, temperature, and lab, it was possible to estimate how much of the difference between the two measures of energy was due to random effects. Comparing the differences of the averaged values (6 tests) tightened the above three levels of agreement to only 3 %, 15 %, and 10 %, respectively. This suggests that most of the differences in the reported energies is systematic rather than random.

A paired-t test was used to determine the statistical significance of the observed differences between encoder/dial and instrumented-striker energies. The paired-t test is ideal since both energy measures come from the same test, and the variance of the difference between the energy pairs is generally much smaller than the variance in the energies themselves. Defining the mean of the energy differences as the mean striker energy minus the mean dial/encoder energy ($\Delta E = E_s - E_d$), then t is defined by:

$$t = \sqrt{n}\,\frac{\Delta E}{s}, \tag{1}$$

where s is the standard deviation of the differences and n is the number of tests per dataset ($n = 6$). The t values for each data set are plotted in Figure 2 as a function of Charpy energy. Each data point is based on the average differences from six duplicate tests by the same laboratory. For 9 out of 19 material/temperature/lab CVN data sets, the average difference in

energy was large enough, compared to the standard deviation of the differences, to conclude with 99 % confidence that there is a systematic difference between the average measured dial energy and the average striker-based energy. Lowering the confidence level to 95 % results in 15 of the 19 CVN data sets being consistent with the premise of systematic differences. For 14 out of the 16 MCVN data sets, it can be concluded with 99 % confidence that there is a systematic difference between the energies measured from the dial and those based on the striker force.

It is very clear from this comparison of dial/encoder and instrumented-striker energies that there are significant systematic differences. There appears to be some bias in the range of less than 40 J towards the instrumented-striker's energy being less than the dial/encoder's energy. This is consistent with there being some residual vibrational energy included in the dial/encoder energies or that additional energy is removed from the pendulum by post-fracture interactions between the specimen and the striker. The significantly larger differences for the MCVN tests could perhaps be the result of their being tested on machines of lower capacities. These machines could possibly be more prone to effects of residual vibrational energy than machines of larger capacities. Assuming that the load-cell strain gages for MCVN testing were placed on the striker in a manner similar to that used in the CVN testing, we would expect that the load distribution effects would be smaller in the MCVN tests due to the smaller contact region (half size). The inertial effects of the striker load-cell would not be expected to be the cause of the large differences in energies, due to the upper-shelf behavior (more plasticity), making the specimen behave in a largely quasi-static manner. However, the effects on the displacement histories (as computed from the striker-load histories) due to the machine's inertia and dynamic response could be greater for the MCNV machines of lower capacity and perhaps relatively less stiffness.

International Comparison of Impact Verification Programs

The keys to achieving reproducible test results that are independent of the machine and the laboratory have been adequate attention to testing-machine maintenance and strict adherence to standard test procedures. The means for ensuring that various Charpy test laboratories can generate comparable results are the four international programs on Charpy-machine certification (described by McCowan et al. [7]). The study described by McCowan et al. is a round robin conducted by these four Charpy certification laboratories. Our original interest in studying these data was rooted in our interest in the differences between the encoder and the instrumented striker data. However, a very interesting finding was made as a result of this study.

Each of the four Participants provided three energy levels of calibration specimens for the study so that there were 12 different specimen groups. Each Participant received 25 specimens from each specimen group. Each Participant tested 15 of each group using a 2 mm striker and the remaining 10 with an 8 mm striker. The certified energy levels ranged from 16.5 J to 258 J. Participant 4 did not provide certified values for their specimens because there were too few specimens to apply their standard certification procedure and still have enough specimens for the round robin. While not explicitly stated by McCowan et al. in their conclusions, each Participant was able to meet the certification standards for each specimen and striker combination for which certified values were determined. In drawing this conclusion, the ISO 148-3 requirements were applied to the specimens of Participants 1 and 2, and ASTM requirements were applied to the specimens of Participant 3. Since Participant 4's specimens did not have certified values, their specimens were not considered in making this

conclusion. If Participant 4's average round-robin test values for its own specimen groups were treated as the certified values, the conclusion would still be that all met the requirements. Interestingly, if the tighter ASTM tolerances at low energies (±1.4 J or 1 ft-lb) were substituted for the ISO requirements (±2 J), two Participants would have failed to match the certified values within required limits on some low-energy specimen groups. Based on the ASTM limits, Participant 4's energies would have been too low on all three combinations of of specimens and strikers combinations, for the low-energy specimen groups 1 and 2 (-1.5 to -1.8 J vs. ±1.4 J limit). Participant 3's energy would have been too high (1.5 J vs. ±1.4 J limit) on the low-energy specimen group 1.

NIST statistics on certification failures show that the low-energy specimens are the most likely to indicate that a test machine does not meet the certification requirements. The combined results for all years show a failure rate of 12.0 % for the low-energy tests, 8.6 % for the high-energy tests, and 9.7 % for the super-high-energy tests. It is interesting to note that the low-energy test shows the largest difference between machines with C-hammer and U-hammer designs, with the U-hammer test machines recording higher energies on average. However, the difference between the medians is only about 0.2 J. It is believed that this small difference is due to the fact that the majority of low-energy test specimens exit the rear of the test machine, which would tend to result in closer agreement between C and U hammers. The NIST records also show that failures at the low-energy level are more often due to energies that are too high relative to the certified value. The asymmetric distribution of the pass-fail data for the low-energy test is shown in Figure 3.

Participant 4's tendency to obtain energies below the certified value is counter to this trend. The information provided by McCowan et al. [7] show that Participant 4 used a machine with a capacity of 500 J, while the rest of the Participants used machines with capacities of 300 to 350 J. They suggested that the use of the higher-capacity machine was the fundamental cause of the lower energies for the low-energy specimens. The basis for this conjecture was the assumption that the higher-capacity machine, due to the greater mass and stiffness of its pendulum and striker, experiences less vibration (and so vibrational energy loss) than the lower-capacity machines.

The data from McCowan et al. was subjected to analysis to determine the statistical significance of the differences in energy measured by the 500 J machine of Participant 4 (relative to the 300/350 J machines of Participants 1, 2, and 3). The large number of duplicate test specimens used in this study, combined with the small coefficient of variation of the specially-manufactured test specimens, makes the data from this study ideal for identifying and studying effects that are normally lost in the scatter of most Charpy-test results. The fact that the data are obtained from perhaps the best-maintained test machines in the world should also not be overlooked.

The standard statistical test for assessing the significance of differences in mean values from two samples is the t test. The approach to applying the t test was to treat each specimen and striker combination as a separate dataset (population). There were 24 such datasets. Since certified values were not available for some datasets, the average results from Participants 1, 2, and 3 were used as the basis for comparison with Participant 4's results. Means (E_{123}) and standard deviations (s_{123}) were computed for the combined data of Participants 1, 2, and 3. Similarly, means (E_4) and standard deviations (s_4) were computed for Participant 4's test results. Then, for each test, the difference in the mean values ($E_4 - E_{123}$) and a pooled standard deviation (s_0) were computed where:

$$s_o^2 = \frac{(n_4 - 1)s_4^2 + (n_{123} - 1)s_{123}^2}{n_4 + n_{123} - 2} \tag{2}$$

and the *n's* are the numbers of specimens in each data set (10 and 30 for the 8 mm striker data sets, or 15 and 45 for the 2 mm striker data sets). A standard deviation computed from the combined data rather than from using a pooled value would overstate the actual variance of the data if there were a significant difference in the means. The t values were computed by:

$$t = \frac{E_4 - E_{123}}{s_o\left(\frac{1}{n_4} + \frac{1}{n_{123}}\right)^{1/2}} \tag{3}$$

Figure 4 shows t as a function of the energy level (E_{123}) for the 24 data sets. Keep in mind that each point represents 60 Charpy tests with a 2 mm striker or 40 tests with an 8 mm striker, and the t test is applied to each of the 24 points (e.g., not to the mean trend of the combined 24 data sets). The statistical significance of the differences in the normalized energy (t) is determined by comparing them to the statistical distribution of t expected if there was no effect of machine capacity on the measured energies (assumes normal distribution and random sampling). The horizontal dashed lines show the expected ranges of t for 70 % and 99 % of the t population if there is no energy difference. For Charpy energies above 40 J, it can be seen that the computed t values are reasonably consistent with the hypothesis that there is no dependence on machine capacity. Below 40 J, the t values are significantly below the expected range, and so it is concluded that there is a very significant difference in the energies measured by the 500 J machine at low Charpy energies.

This statistical test has therefore shown that the -2 % to -9 % difference in energy (average –6.2 %) of the 500 J machine at the lower Charpy energies is not due to random effects. It was originally postulated that this systematic effect was due to residual vibrational energy. However, the accelerometer experiments described above and the numerical simulations of [1] could explain only differences of 1 to 2 %. Calculations performed in this study using a simple two-mass, two-spring model of the specimen and striker system suggest that the energy difference can be explained in terms of a frequency shift in the applied load caused by a stiffer design of the striker assembly in the 500 J machine. The frequency at which the specimen and striker vibrate during the initial elastic loading is affected by the specimen's stiffness (k_s) and mass (m_s) as well as the stiffness of the striker assembly (k_h) according to

$$f = (1/2\pi)\sqrt{(k_s + k_h)/m_s}\ . \tag{4}$$

The mass of the striker assembly (m_h) is essentially infinite with respect to that of the specimen and therefore does not affect the frequency behavior of interest. As shown in Figure 5, a 20 % higher stiffness for the striker assembly results in a 7 % increase in the natural frequency of the specimen and striker assembly system. The higher frequency causes the critical fracture load to be reached at a smaller displacement of the specimen, which in turn, requires less absorbed energy to fracture the specimen. These findings suggest not only that the observed low-energy measurements could be the function of the test-machine design, but more importantly, that the test machine could be interacting with the specimen to materially affect the fracture behavior of the specimen.

SUMMARY

Numerical simulations and experimentation have demonstrated the potential for significant losses in energy due to vibration in Charpy test machines. For the 400 J U-hammer machine considered in this study, the vibrational energy is estimated to be on the order of 1 % of the Charpy test energy. While the vibrational energy is significant, it is not sufficient to explain the differences between dial and instrumented energies (on the order of 2 % to 20%) that are observed when testing low-energy specimens that exit the front of the test machine. These larger differences can be explained by the post-fracture interactions that are observed between the striker and the specimen. Measurements performed during the current study showed that the post-fracture impacts with the striker add an average of 3 to 4.5 J to the dial energy. Thus, the post-fracture interactions between the specimen and striker can account for a large share of the energy differences between the dial and the instrumented-striker energies. Other effects that add to the energy difference include: load distribution in the striker; test machine inertia, striker inertia; and windage and friction correction of the dial.

For the low-energy specimens of the international round robin reported by McCowan et al. [7], the 500 J capacity machine gave energies that were 2 to 9 % less than those measured using 300 to 350 J machines. It was originally postulated that this systematic effect was due mostly to residual vibrational energy in the test machine. However, experimental and numerical studies of vibrational energy on test machines have been unable to explain more than a difference of 1 to 2 %. The simple two-mass, two-spring dynamic model of this study has shown that a change of 20 % in the stiffness of the striker assembly can lead to a difference in absorbed energy of about 9 % in low-energy Charpy specimens. Therefore, it now appears that the observed energy difference of 2 to 9 % could be due to a stiffer design of the striker assembly for the 500 J machine. The mechanism for this difference in energy is that increasing the stiffness of the striker assembly increases the frequency of the inertial peaks during the elastic portion of the specimen's response. This higher frequency results in the critical fracture load being reached at a smaller displacement, which in turn, results in lower absorption of energy before fracture. These findings are potentially important because they suggest that the energy to fracture low-energy specimens is dominated by the design of the test machine.

REFERENCES

1. Manahan, M. P., Sr., and Stonesifer, R. B., **"The Difference Between Total Absorbed Energy Measured Using An Instrumented Striker and That Obtained Using an Optical Encoder,"** *Pendulum Impact Testing: A Century of Progress, STP 1380*, T. A. Siewert and M. P. Manahan, Sr., Eds., American Society for Testing and Materials, West Conshohocken, PA, 2000, pp. 181-197.

2. Kobayashi, T., Inoue, N., Morita, S., and Toda, H., **"On the Accuracy of Measurement and Calibration of Load Signal in the Instrumented Charpy Impact Test,"** *Pendulum Impact Testing: A Century of Progress, STP 1380*, T. A. Siewert and M. P. Manahan, Sr., Eds., American Society for Testing and Materials, West Conshohocken, PA, 2000, pp 198-209.

3. Kalthoff, J. F., van Walle, E., and Wilde, G., "**Variations of the sensitivity of instrumented ISO/DIN and ASTM tups and their influence on the determination of impact energies in tests with ductile steels**," *Evaluating Material Properties by Dynamic Testing*, ESIS 20 (Edited by E. van Walle), Mechanical Engineering Publications, London, 1996, pp. 25-35.

4. Winkler, S. and Voβ, B., "**Static force calibration of Charpy impactors**," *Evaluating Material Properties by Dynamic Testing*, ESIS 20 (Edited by E. van Walle), Mechanical Engineering Publications, London, 1996, pp. 37-44.

5. Manahan, M. P., Sr., and Stonesifer, R. B., **"Studies Toward Optimum Instrumented Striker Designs,"** to appear elsewhere in these proceedings.

6. Manahan, M. P., Sr., Martin, F. J., and Stonesifer, R. B., **"Results of the ASTM Instrumented/Miniaturized Round Robin Test Program,"** *Pendulum Impact Testing: A Century of Progress, STP 1380*, T. A. Siewert and M. P. Manahan, Sr., Eds., American Society for Testing and Materials, West Conshohocken, PA, 2000, pp 223-241.

7. McCowan, C. N., Pauwels, J., Revise, G., and Nakano, H., **"International Comparison of Impact Verification Programs,"** *Pendulum Impact Testing: A Century of Progress, STP 1380*, T. A. Siewert and M. P. Manahan, Sr., Eds., American Society for Testing and Materials, West Conshohocken, PA, 2000, pp 73-89.

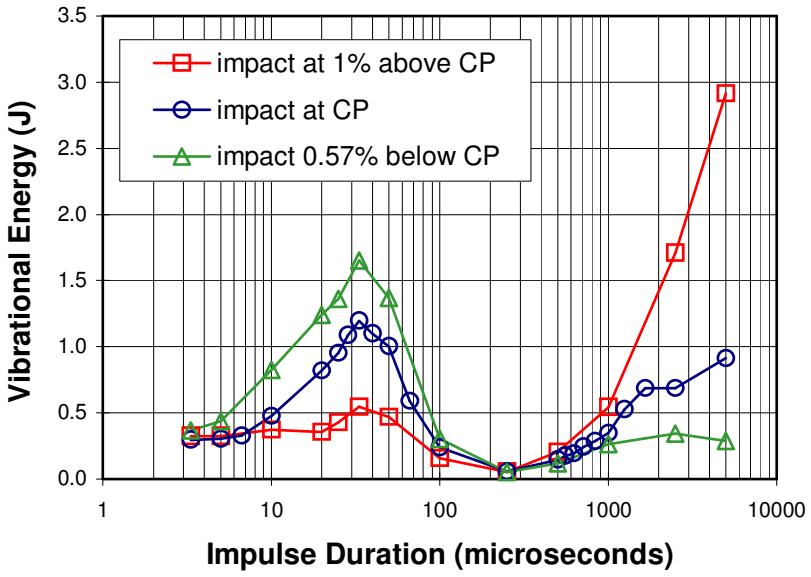

Figure 1 **Residual Vibrational Energy in the Pendulum for Various Idealized Impulses (Fmax = 620 kN) and Strike Locations.**

Table 1 Summary of Estimates of Pendulum Vibrational Energy from Analysis of Pendulum Acceleration Data.

Specimen Type	Charpy Energy (J)	Vibrational Energy (J)	Vibrational Energy (%)	Peak Energy Frequency (cps)
		Lateral Vibration Model of Tube		
super-high-energy	227.7	0.47	0.2	136
High-energy	131.9	0.35	0.3	136
Low-energy	23.0	0.16	0.7	1224
		Angular Vibration Model of Hammer		
super-high-energy	211.8	2.02	1.0	136
High-energy	131.0	0.95	0.7	136
Low-energy	22.3	0.15	0.7	2175

Table 2 Energy Results from Optical Encoders for Impact Tests Conducted Simultaneously with High-speed Photography. Tests conducted at 20 °C.

Specimen Exited Rear of Test Machine			Specimen Exited Front of Test Machine		
ID LL1-	Energy (J)	Striker Contact	ID LL1-	Energy (J)	Striker Contact
219	18.1	No	204	20.9	Yes
36	18.0	1 hit	65	19.7	Yes
23	18.0	1 hit	201	19.1	Yes
-	-	-	194	21.9	Yes
-	-	-	279	22.0	Yes
-	-	-	187	23.1	Yes
-	-	-	61	26.3	Yes
-	-	-	234	19.2	Yes
-	-	-	5	19.1	Yes
-	-	-	97	19.0	Yes
-	-	-	235	18.6	Yes
-	-	-	81	19.3	Yes
-	-	-	202	23.6	Yes
Average	18.0	-	Average	20.9	-
Std. Dev.	0.1	-	Std. Dev.	2.3	-

Table 3 Energy Results from Optical Encoders for Impact Tests Conducted Simultaneously with High-speed Photography. Tests conducted at -40 °C.

Specimen Exited Rear of Test Machine			Specimen Exited Front of Test Machine		
ID LL1-	Energy (J)	Striker Contact	ID LL1-	Energy (J)	Striker Contact
250	16.2	No	73	19.7	Yes
252	15.5	No	126	18.2	Yes
182	17.2	No	15	21.3	Yes
242	18.9	1 hit	240	23.3	Yes
63	18.2	No	222	27.0	Yes
-	-	-	119	18.5	Yes
-	-	-	39	24.6	Yes
Average	17.2	-	Average	21.8	-
Std. Dev.	1.4	-	Std. Dev.	3.3	-

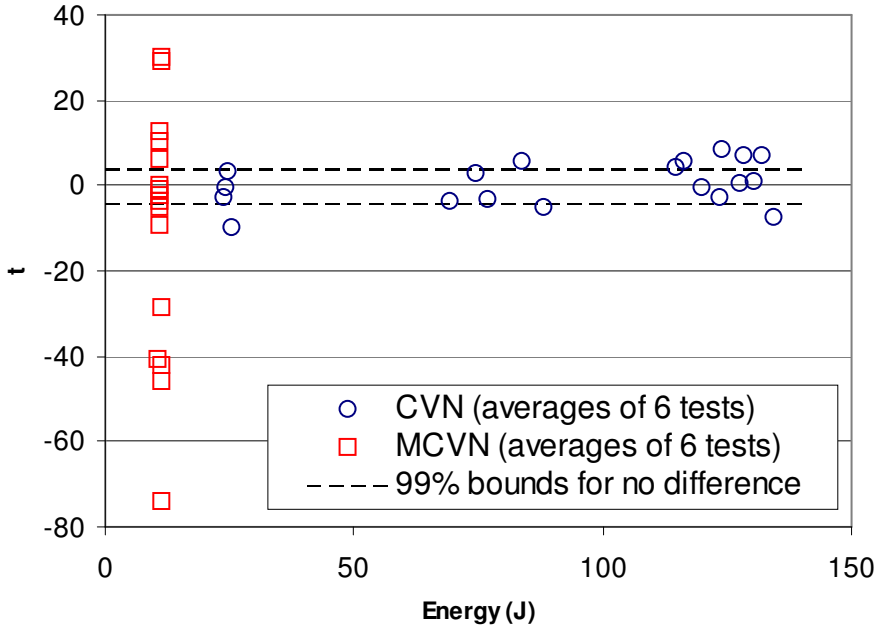

Figure 2 **Test Statistic t for Differences Between Energies from Instrumented-strikers and Dial/Encoders (ASTM Round Robin).**

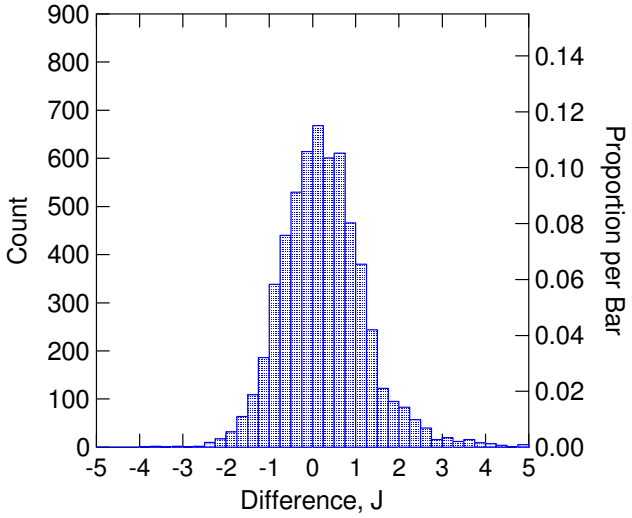

Figure 3 **Asymmetric Pass-Fail Distribution for NIST Low-energy Test (the pass-fail criterion is a difference of 1.4 J).**

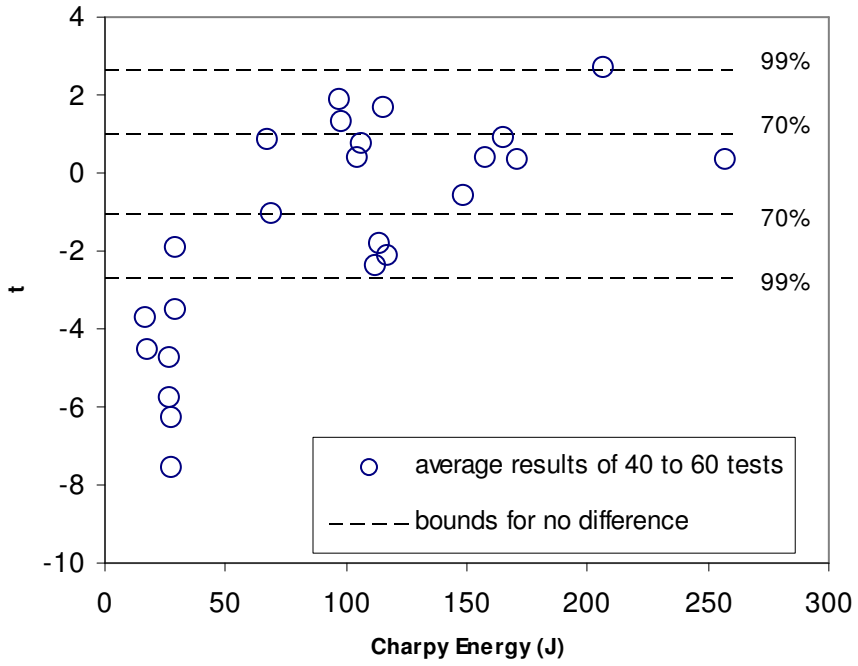

Figure 4 **Test Statistic t for Measured Energy Differences Between the 500 J Capacity Machine and the Average Energies from the 300 to 350 J Capacity Machines.**

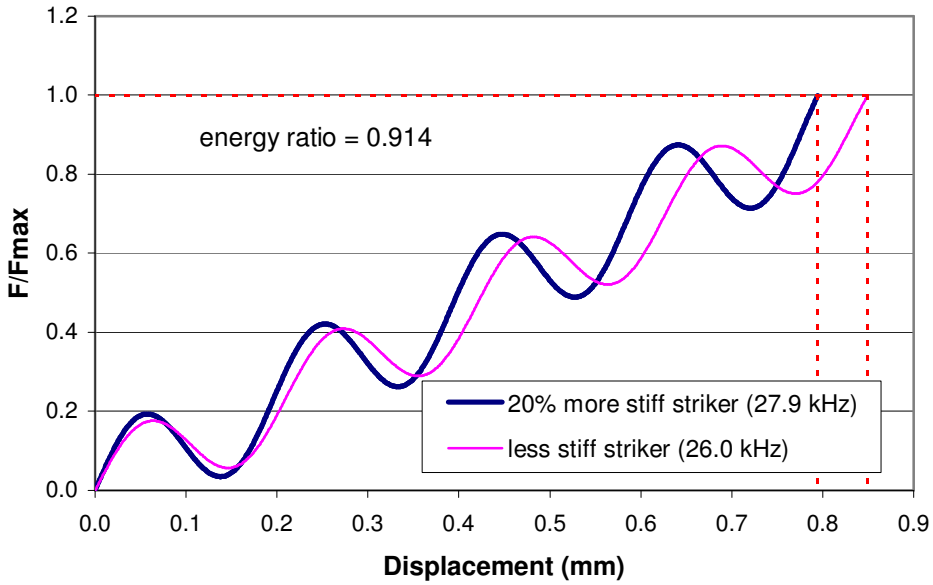

Figure 5 **Results of Two-Mass, Two-Spring Models to Determine the Effect of Stiffening the Pendulum on the Absorbed Energy.**